LETTERS

Obliquity-paced Pliocene West Antarctic ice sheet oscillations

T. Naish[1,2], R. Powell[3], R. Levy[4]†, G. Wilson[5], R. Scherer[3], F. Talarico[6], L. Krissek[7], F. Niessen[8], M. Pompilio[9], T. Wilson[7], L. Carter[1], R. DeConto[10], P. Huybers[11], R. McKay[1], D. Pollard[12], J. Ross[13], D. Winter[4], P. Barrett[1], G. Browne[2], R. Cody[1,2], E. Cowan[14], J. Crampton[2], G. Dunbar[1], N. Dunbar[13], F. Florindo[15], C. Gebhardt[8], I. Graham[2], M. Hannah[1], D. Hansaraj[1,2], D. Harwood[4], D. Helling[8], S. Henrys[2], L. Hinnov[16], G. Kuhn[8], P. Kyle[13], A. Läufer[17], P. Maffioli[18], D. Magens[8], K. Mandernack[19], W. McIntosh[13], C. Millan[7], R. Morin[20], C. Ohneiser[5], T. Paulsen[21], D. Persico[22], I. Raine[2], J. Reed[23,4], C. Riesselman[24], L. Sagnotti[15], D. Schmitt[25], C. Sjunneskog[26], P. Strong[2], M. Taviani[27], S. Vogel[3], T. Wilch[28] & T. Williams[29]

Thirty years after oxygen isotope records from microfossils deposited in ocean sediments confirmed the hypothesis that variations in the Earth's orbital geometry control the ice ages[1], fundamental questions remain over the response of the Antarctic ice sheets to orbital cycles[2]. Furthermore, an understanding of the behaviour of the marine-based West Antarctic ice sheet (WAIS) during the 'warmer-than-present' early-Pliocene epoch (~5–3 Myr ago) is needed to better constrain the possible range of ice-sheet behaviour in the context of future global warming[3]. Here we present a marine glacial record from the upper 600 m of the AND-1B sediment core recovered from beneath the northwest part of the Ross ice shelf by the ANDRILL programme and demonstrate well-dated, ~40-kyr cyclic variations in ice-sheet extent linked to cycles in insolation influenced by changes in the Earth's axial tilt (obliquity) during the Pliocene. Our data provide direct evidence for orbitally induced oscillations in the WAIS, which periodically collapsed, resulting in a switch from grounded ice, or ice shelves, to open waters in the Ross embayment when planetary temperatures were up to ~3 °C warmer than today[4] and atmospheric CO_2 concentration was as high as ~400 p.p.m.v. (refs 5, 6). The evidence is consistent with a new ice-sheet/ice-shelf model[7] that simulates fluctuations in Antarctic ice volume of up to +7 m in equivalent sea level associated with the loss of the WAIS and up to +3 m in equivalent sea level from the East Antarctic ice sheet, in response to ocean-induced melting paced by obliquity. During interglacial times, diatomaceous sediments indicate high surface-water productivity, minimal summer sea ice and air temperatures above freezing, suggesting an additional influence of surface melt[8] under conditions of elevated CO_2.

The Earth's climate system during the Pliocene and early-Pleistocene epochs was regulated by a ~40-kyr periodicity. The geological evidence for this is widespread and expressed in polar to equatorial depositional environments including (1) ice volume from oxygen isotope ($\delta^{18}O$) records, that co-vary with the pattern of ice-rafted debris in deep-sea sediments[9]; (2) ocean circulation[10] and temperature also inferred from deep-sea sediment proxies[11,12]; (3) atmospheric circulation from continental dust deposits[13]; and (4) global sea-level fluctuations recorded in the shallow-marine continental margins[14].

The 40-kyr cycle is almost certainly linked to variations in the Earth's orbital obliquity. However, the specific nature of this forcing and its influence on Antarctic glaciation remain unresolved owing to a lack of well-dated climate records that directly sample past oscillations of the ice sheet. The new AND-1B core provides such a record (Fig. 1). In this Letter, we focus on the early Pliocene (~5–3 Myr ago) part of the record, because for this period the response of Antarctic ice sheets to orbital forcing can be studied without the complicating influence of large Northern Hemisphere ice sheets on sea-level and deep-sea $\delta^{18}O$ records[15]. Furthermore, polar ice-sheet boundary conditions were similar to today, but the climate was warmer[3,5,6]. With anthropogenic warming projected to rise an average of ~3 °C in mean temperature by the end of the twenty-first century, more significance is being placed on the early Pliocene as an analogue for understanding the future behaviour of the WAIS[3] and its contribution to global sea level[16]. Far-field geological evidence for palaeoshorelines up to 25 m above present[17,18] are consistent with ice-volume estimates from deep-ocean $\delta^{18}O$ data[19], and imply deglaciation of the Greenland ice sheet, the

[1]Antarctic Research Centre, Victoria University of Wellington, Kelburn Parade, PO Box 600, Wellington 6012, New Zealand. [2]GNS Science, 1 Fairway Drive, PO Box 30-368, Lower Hutt 5040, New Zealand. [3]Department of Geology & Environmental Geosciences, Northern Illinois University, DeKalb, Illinois 60115, USA. [4]ANDRILL Science Management Office, Department of Geosciences, University of Nebraska-Lincoln, Lincoln, Nebraska 68588-0340, USA. [5]University of Otago, Department of Geology, PO Box 56, Leith Street, Dunedin, Otago 9001, New Zealand. [6]Università di Siena, Dipartimento di Scienze delle Terra, Via Laterina 8, I-53100 Siena, Italy. [7]Ohio State University, Department of Geological Sciences, 275 Mendenhall Lab, 125 South Oval Mall, Columbus, Ohio 43210, USA. [8]Alfred Wegener Institute, Department of Geosciences, Postfach 12 01 6, Am Alten Hafen 26, D-27515 Bremerhaven, Germany. [9]Istituto Nazionale di Geofisica e Vulcanologia, Via della Faggiola 32, I-56126 Pisa, Italy. [10]Department of Geosciences, 233 Morrell Science Centre, University of Massachusetts, Amherst, Massachusetts 01003-9297, USA. [11]Department of Earth and Planetary Sciences, Harvard University, Massachusetts 02138, USA. [12]Earth and Environmental Systems Institute, Pennsylvania State University, University Park, Pennsylvania 16802, USA. [13]New Mexico Institute of Mining & Technology, Earth & Environmental Sciences, Socorro, New Mexico 87801, USA. [14]Department of Geology, Appalachian State University, ASU Box 32067, Boone, North Carolina 28608-2067, USA. [15]Istituto Nazionale di Geofisica e Vulcanologia, Via di Vigna Murata 605, I-00143 Rome, Italy. [16]Department of Earth and Planetary Sciences, Johns Hopkins University, Baltimore, Maryland 21218, USA. [17]Federal Institute of Geosciences & Natural Resources, BGR, Stilleweg 2, D-30655 Hannover, Germany. [18]Università Milano-Bicocca, Dipartimento di Scienze Geologiche e Geotecnologie, Piazza della Scienza 4, I-20126 Milano, Italy. [19]Colorado School of Mines, Department of Chemistry & Geochemistry, 1500 Illinois Street, Golden, Colorado 80401, USA. [20]US Geological Survey, Mail Stop 403, Denver Federal Center, Denver, Colorado 80225, USA. [21]University of Wisconsin-Oshkosh, Department of Geology, 800 Algoma Boulevard, Oshkosh, Wisconsin 54901, USA. [22]Dipartimento di Scienze della Terra, Università degli Studi di Parma, Via Usberti 157/A, I-43100 Parma, Italy. [23]CHRONOS, Iowa State University, Department of Geological & Atmospheric Sciences, 275 Science I, Ames, Iowa 50011-3212, USA. [24]Department of Geological and Environmental Sciences, School of Earth Sciences, Stanford University, Stanford, California 94305, USA. [25]Department of Physics, Mailstop #615, University of Alberta, Edmonton, Alberta T6G 2G7, Canada. [26]Department of Geology and Geophysics, Louisiana State University, Baton Rouge, Louisiana 70803, USA. [27]CNR, ISMAR – Bologna, Via Gobetti 101, I-40129 Bologna, Italy. [28]Albion College, Department of Geology, Albion, Michigan 49224, USA. [29]Columbia University, Lamont-Doherty Earth Observatory, Palisades, New York 10964, USA. †Present address: GNS Science, 1 Fairway Drive, PO Box 30368, Lower Hutt 5040, New Zealand.

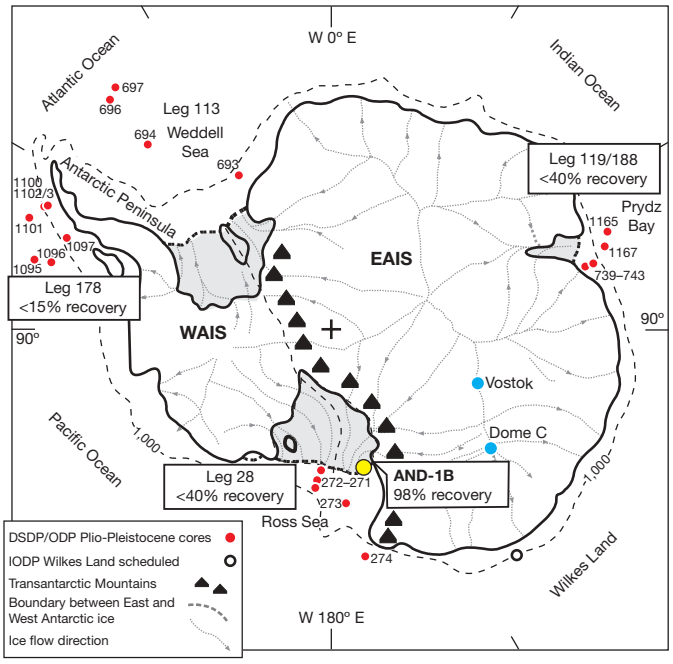

Figure 1 | Location of the ANDRILL McMurdo Ice Shelf Project AND-1B drill site in the northwestern corner of the Ross ice shelf. Also shown are the locations of previous Deep Sea Drilling Project (DSDP), Integrated Ocean Drilling Program (IODP) and Ocean Drilling Program (ODP) cores, Plio-Pleistocene cores, percentage recovery (from shelf sites) and geographic features including ice-sheet configuration and flow lines. (Supplementary Figs 1 and 2 show more detail of the glaciologic and geologic setting). The dashed contour indicates a depth of 1,000 m below sea-level.

WAIS and the marine margins of the East Antarctic ice sheet (EAIS) during the warmest early Pliocene interglacials.

Thirty-eight glacimarine cycles, each bounded by glacial surfaces of erosion (GSEs), occur in the upper 600 m of the core, and record oscillations in the extent of an ice sheet in Ross embayment during the past 5 Myr (Fig. 2)[20]. The drilled strata accumulated in the rift axis of the Victoria Land basin, ~100 km seaward of the coast. Accommodation space for the preservation of the sediments, and their protection from subsequent glacial erosion, was provided by high rates of tectonic subsidence due to a unique combination of regional rift extension and flexure of the crust by local volcanic islands (Supplementary Information).

Figures 3 and 4 summarize our interpretations of individual sedimentary cycles in terms of the vertical occurrences of lithofacies, that is, sediments representing specific environments of deposition. These range from marine-diatom-rich deposits and mudstones deposited during interglacials to ice-proximal diamictites, conglomerates and sandstones representing glacial periods. During glacial periods, the ice sheet had a laterally extensive marine terminus extending well beyond the drill site, out into the Ross Sea. During interglacials, the drill site was either covered by an ice shelf or, when the ice sheet retreated, lay in open water. The sedimentary characteristics of the cycles and the approach used for their interpretation are given in more detail elsewhere[21] (Methods). We note here that changes in lithofacies through time primarily reflect the proximity of the ice-sheet grounding zone and the thermal characteristics of the depositing ice (Fig. 2 and Supplementary Information). Such inferences are consistent with depositional models from a variety of different glacimarine regimes[22,23], and permit the identification of 38 oscillations in the extent of the ice sheet's grounding line.

The composition of till (ice-contact diamictites), which overlie GSEs and represent sediments transported at the base of a grounded ice sheet, show that the ice originated from large outlet glaciers in the Transantarctic Mountains (TAM), especially the Mulock and Skelton glaciers south of Minna Bluff[21]. A new continental Antarctic ice-sheet model[7] run for the past 5 Myr supports geological interpretations that the provenance of grounded ice at the AND-1B site is always from nearby southern-TAM outlet glaciers during glacial advances (Fig. 2).

Notably, the model finds that local ice variations at the AND-1B site are indicative of the overall West Antarctic glacial state, because both are controlled by variations in ocean-induced melt. When open-water marine sediments occur in the AND-1B core, the model shows not only deglaciation in the western Ross embayment, but also the collapse of the entire WAIS (Fig. 2). Pliocene–Pleistocene variations in ice volume are dominated by large WAIS advances and retreats, while the high-altitude regions of the EAIS remain relatively stable. This is because air temperatures never become warm enough to cause significant surface melting on the EAIS[24], whereas variations in ocean-induced melt and sea level affect the marine-based WAIS much more than the EAIS. Thus, the sedimentary cycles in the AND-1B core both track local variations of the coastal margin of the EAIS (for example TAM outlet glaciers) and provide physical evidence for major changes in the mass balance of the WAIS (Supplementary Information).

Figure 2 illustrates the stratigraphic position of 26 chronological datums that are used to constrain the age and duration of the 38 sedimentary cycles and identify the time missing at cycle-bounding erosion surfaces, that is, unconformities (Supplementary Table 1). The chronology is developed from $^{40}Ar/^{39}Ar$ ages of volcanic deposits and a quantitative diatom biostratigraphy used to constrain the correlation between the magnetic polarity stratigraphy and the geomagnetic polarity timescale[21]. The approach used, and associated uncertainties, are outlined in Methods. About 36% of the last 5 Myr is represented as rock in the AND-1B core; the rest is lost at unconformities resulting from erosion through long-term tectonic influences and shorter-term volcanic and glacial processes. Chronostratigraphic constraints enable identification of two types of unconformities: (1) those where the time missing is longer than a Milankovitch cycle, interpreted as major erosion due to tectonic influences and/or a major phase of glacial advance; and (2) those of suborbital duration reflecting lesser glacial erosion associated with a single glacial advance truncating only part of the previous cycle. The chronology also allows the duration of relatively continuous stratigraphic packages comprising more than one cycle to be estimated with sufficient precision for the recognition of orbital periods[25] (Methods).

One such interval is illustrated in detail in Fig. 3 and comprises six early-Pliocene glacial cycles (cycles 38–33), spanning 265 kyr. In this case, the identification of three palaeomagnetic reversal boundaries allows one-to-one matching of the WAIS grounding-line oscillations recorded in the AND-1B core to individual 40-kyr ice-volume cycles in the deep-sea benthic $\delta^{18}O$ stack[26] and modelled ice-volume cycles between 4.896 and 4.631 Myr ago. Figure 4 illustrates an interval in which the chronology constrains 16 successive early- to mid-Pliocene (3.60–2.87 Myr ago) cycles (32a–d to 20), spanning 700 kyr. In this case, the cyclostratigraphic interpretation and the distribution of time within the AND-1B core are not so straightforward, primarily because a ~60-m-thick interval of marine diatomite, spanning ~200 kyr, occurs between 438 and 376 m.b.s.f. We use the distribution of >2-mm-diameter iceberg-rafted debris (IBRD) through the continuous, thick diatomite unit as an index for ice-rafting intensity and glacial variability. The IBRD record identifies four or five main orbital cycles (32a–d) reflecting glacial fluctuations during an extended period of biopelagic deposition in the Ross embayment, when the ice sheet remained landward of the drill site (Fig. 2). The composition of the IBRD reflects oscillations of local outlet glaciers, which remained near the coast with no significant expansion into the Ross Sea[21].

If the four or five IBRD cycles in the diatomite and the eleven overlying unconformity-bounded cycles are distributed evenly over this time interval, the resulting duration is ~40 kyr per cycle (Fig. 4).

The short-duration normal-polarity interval between the Mammoth and Kaena subchrons is not represented in the AND-1B core and could be missing at any of the GSEs between the bases of cycles 28–22. However, if cycles 28–22 are distributed evenly across the amalgamated reversed-polarity subchrons between 3.30 and 3.03 Myr ago, then a one-to-one match with ~40-kyr $\delta^{18}O$ cycles results and suggests that an intervening normal-polarity interval is most likely missing at the basal GSE of cycle 26.

The 60-m-thick diatomite unit lacks a sea-ice-associated diatom flora[27], and sedimentological evidence implies that warmer-than-present

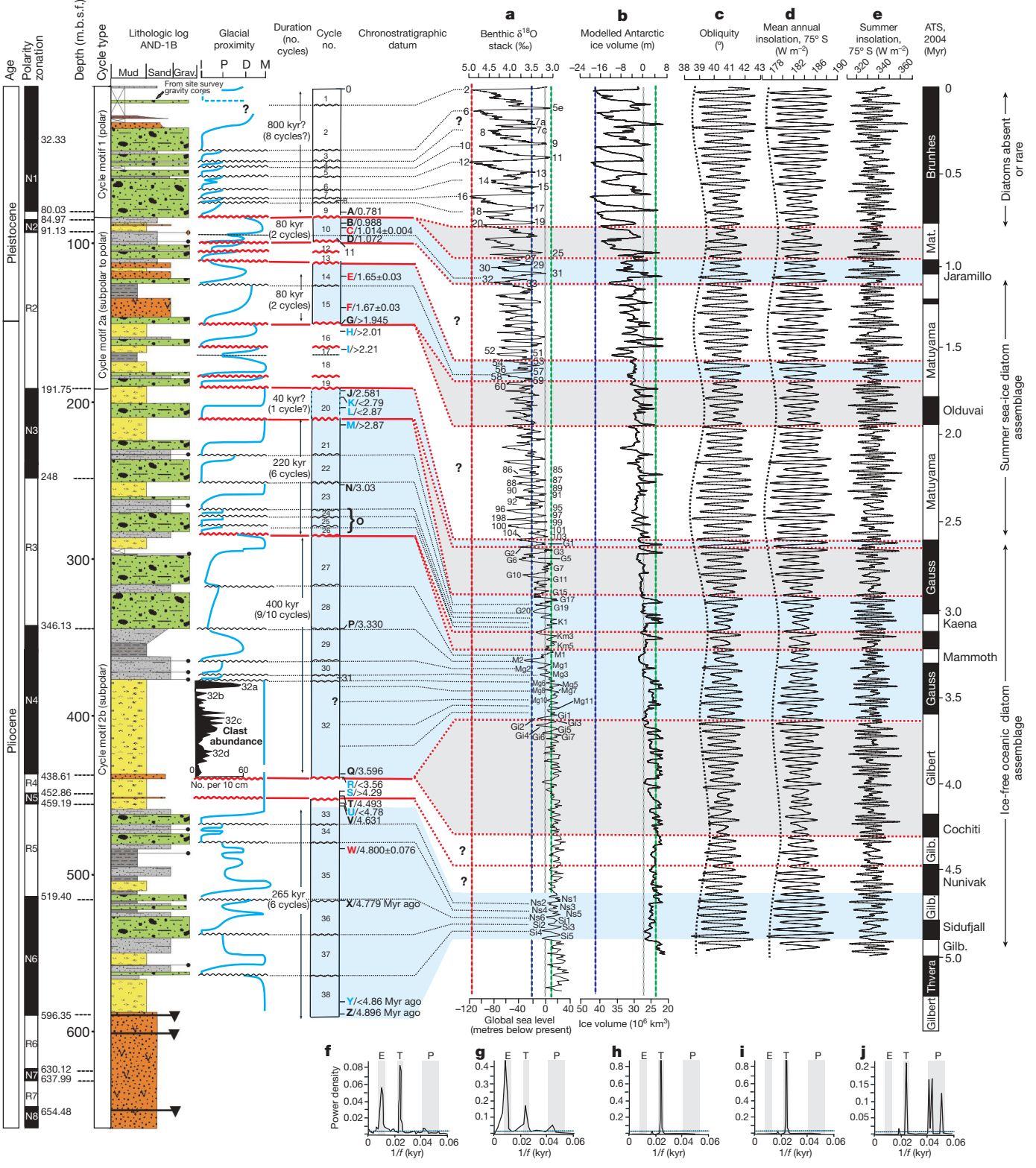

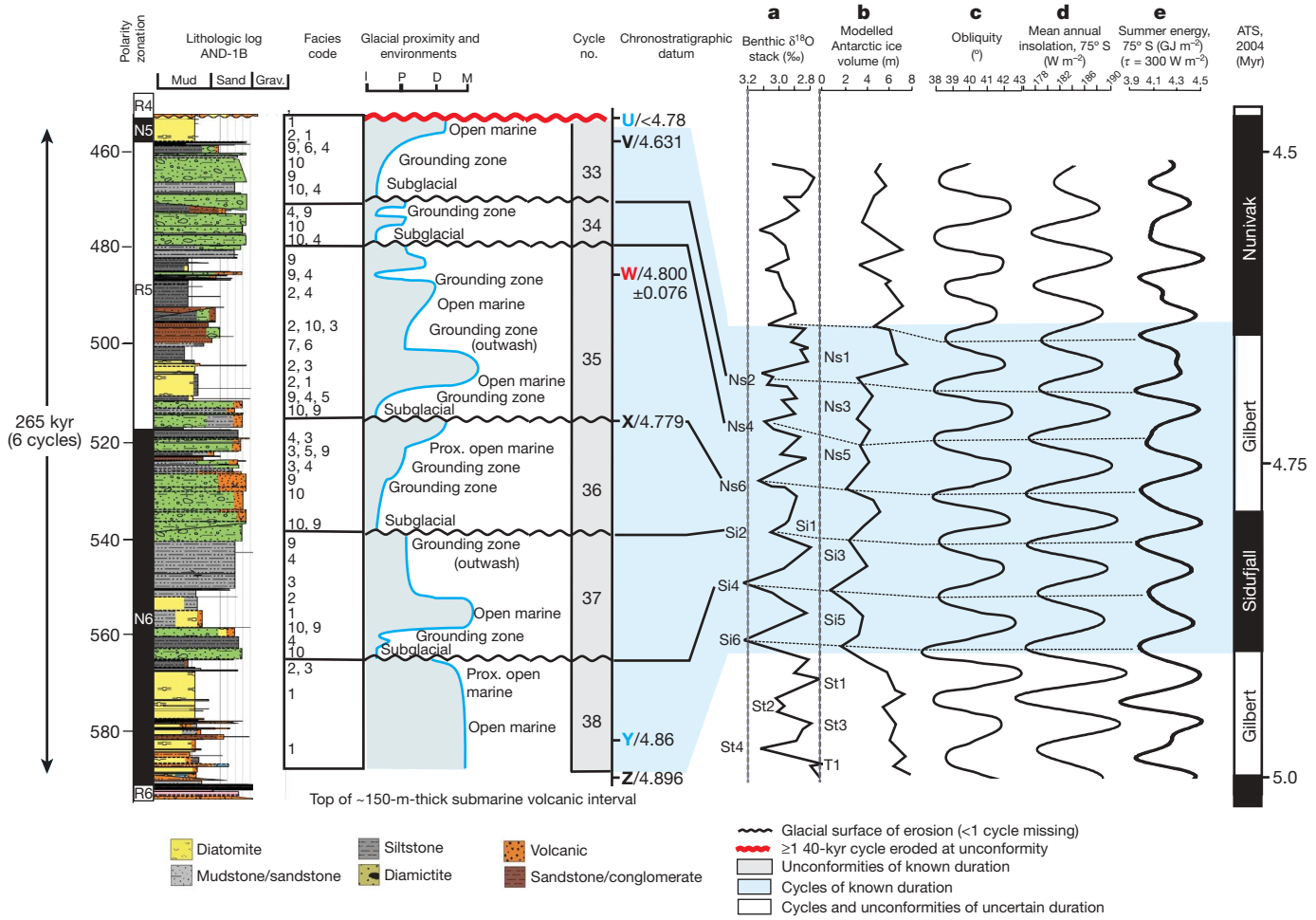

Figure 3 | Detailed analysis of early-Pliocene sedimentary cycles in the AND-1B core showing lithofacies interpretations of glacimarine environments. The glacial proximity curve tracks the relative position of the grounding line through ice-contact (I), ice-proximal (P), ice-distal (D) and marine (M) environments and provides a proxy for ice-sheet extent. Cycle duration is constrained by chronostratigraphic datums coded A–Z. The chronostratigraphy allows a one-to-one correlation of the cycles with obliquity-paced time series of the benthic $\delta^{18}O$ record[26] (**a**), modelled Antarctic ice volume[7] (expressed in metres of equivalent sea level, **b**), obliquity (**c**), mean annual insolation at 75° S (**d**), and summer energy at 75° S for inferred melt threshold (τ) of 300 W m^{-2} (**e**; see Supplementary Information for further explanation of summer energy). Dashed vertical lines represent present-day ice volume/sea level. (See Methods and Supplementary Table 2 for explanation of facies codes.)

oceanic and atmospheric conditions existed between ~3.6 and 3.4 Myr ago. Foraminiferal $\delta^{18}O$ values during this time are up to 0.4‰ lower than during the Holocene epoch, with amplitudes of 0.15 to 0.35‰ equivalent to eustatic sea-level fluctuations (including Northern Hemisphere ice; see Methods) of +10–30 m. Modelled Antarctic ice volume reduces to 20×10^6 km^3, or +7 m in equivalent sea level (Fig. 2), and involves the complete deglaciation of WAIS together with a loss of up to +3 m in equivalent sea level (5%) from the marine margins of the EAIS[7]. If complete deglaciation of Greenland (+5 m) also occurred during this time, then the Antarctic ice-sheet history from isotopes, proximal data and numerical models is in good agreement with the early-Pliocene eustatic sea-level fluctuation amplitudes of +10–30 m reconstructed from far-field sites such as the uplifted shallow-marine Wanganui basin (New Zealand)[18].

The WAIS grounding line re-advanced across the western Ross Sea following deposition of the thick diatomite interval, as shown by the occurrence of progressively more ice-proximal facies in the core between sedimentary cycles 31 and 29 (Fig. 4). The interval is correlated with a 0.7‰ increase in $\delta^{18}O$ between marine isotope stages Mg5 and M2, and a corresponding increase in modelled Antarctic ice volume equivalent to a eustatic fall from 7 m above present-day sea level to 1 m below[7]. The M2 glacial appears to terminate early-Pliocene warm conditions in the Ross embayment. Our glacial proximity curve shows that WAIS expansion across the drill site occurred during the early

Figure 2 | Stratigraphic and chronologic summary of the upper 600 m of the AND-1B core showing 38 sedimentary cycles of ice-sheet advance, retreat and re-advance during the last 5 Myr. Lithologies (rock types) are plotted against depth. The glacial proximity curve tracks the relative position of the grounding line through ice-contact (I), ice-proximal (P), ice-distal (D) and marine (M) environments and provides a proxy for ice-sheet extent. Cycle duration is constrained by chronostratigraphic datums coded A–Z (Supplementary Table 1) and is explained in more detail in Methods. The chronostratigraphy allows correlation of some cycles (blue shading) with time series of the stacked benthic $\delta^{18}O$ record[26] ($\delta^{18}O = (^{18}O/^{16}O)_{sample}/(^{18}O/^{16}O)_{SMOW} - 1$; SMOW, standard mean ocean water; **a**), model-output Antarctic ice volume[7] (expressed in metres of equivalent sea level, **b**), obliquity (**c**), mean annual insolation at 75° S (**d**) and summer insolation intensity at 75° S (**e**). Spectral estimates show that the majority of the variance is at ~40-kyr frequency for the $\delta^{18}O$ record (**f**), obliquity (**h**) and mean annual insolation (**i**). Summer insolation at 75° S has equal power in the obliquity and precession bands (**j**). The relative increase in 100-kyr power in model-output Antarctic ice volume (**g**) reflects the increased influence of large Northern Hemisphere ice sheets on ocean temperature and glacioeustatic fluctuations in the late Pleistocene. In **f**–**j**: E, eccentricity or ~100-kyr cycle of unknown origin; T, tilt (obliquity); P, precession; *f*, frequency; vertical axes, power as an arbitrary scale of relative spectral power. m.b.s.f., metres below sea floor; LGM, Last Glacial Maximum. Thin diamictites (<3 m) are represented by a horizontal line with dot at end.

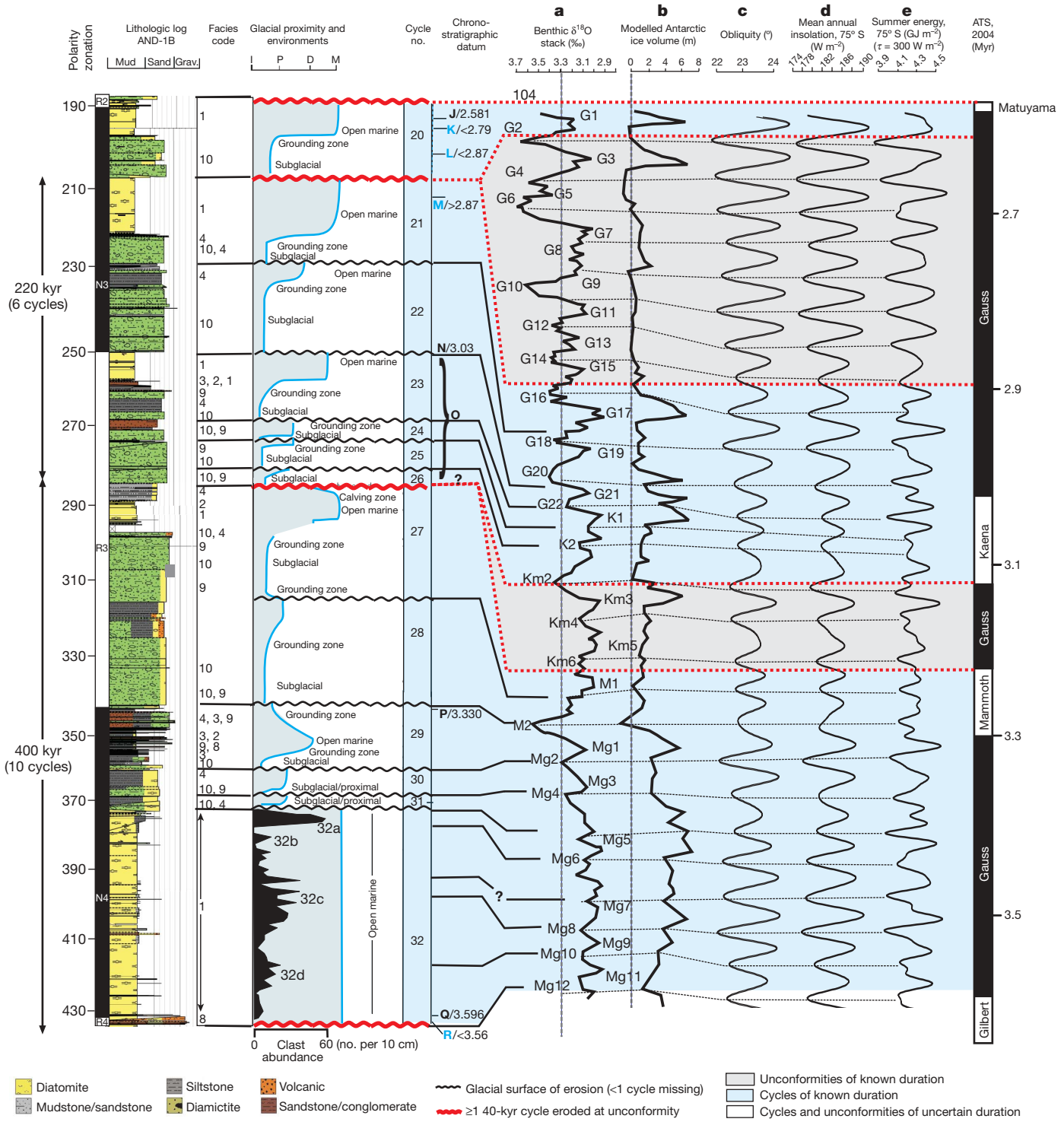

Figure 4 | Detailed analysis of late early-Pliocene sedimentary cycles in the AND-1B core showing lithofacies interpretations of glacimarine environments. Glacial proximity curve tracks the relative position of the grounding line through ice-contact (I), ice-proximal (P), ice-distal (D) and marine (M) environments and provides a proxy for ice-sheet extent. Cycle duration is constrained by chronostratigraphic datums coded A–Z. The chronostratigraphy allows recognition of 15 cycles, within a ~600-kyr period, that are correlated with obliquity-paced time series of the benthic $\delta^{18}O$ record[26] (**a**), modelled Antarctic ice volume[7] (**b**), obliquity (**c**), mean annual insolation at 75° S (**d**) and summer energy at 75° S for $\tau = 300$ W m^{-2} (**e**). Dashed vertical lines represent present-day ice volume/sea level.

Pliocene when Holocene $\delta^{18}O$ values and present-day Antarctic ice volumes (27×10^6 km^3) were exceeded. An up-core transition between 350 and 150 m.b.s.f. is evident, marked by successively fewer submarine outwash deposits and thinner grounding-zone facies successions representing cooling of the ice sheet implied by progressively lower volumes of melt water (Supplementary Information and ref. 21). This culminates with a major cooling step that occurs across the Gauss–Matuyama polarity transition (2.6 Myr ago) associated with significant erosion and loss of the late-Pliocene stratigraphic record (Fig. 2). This step is taken to represent a major expansion of the ice sheet.

The ~40-kyr-year variability in the size of the WAIS suggests differences from Milankovitch's hypothesis that summer half-year insolation intensity, with its sensitivity to precession (Fig. 2e), should control the growth and decay of ice sheets. Historically, the lack of

precession in the geological record has been attributed to the importance of annual insolation that is controlled by obliquity, with more influence on polar temperatures than seasonal insolation modulated by precession (see, for example, ref. 28). Figure 2 highlights the relationship between obliquity (Fig. 2c), mean annual insolation (Fig. 2d) and the AND-1B cycles for the Pliocene, and Figs 3 and 4 show details for the early Pliocene. Given the sensitivity of WAIS mass balance to ocean temperature[7], we suggest that 40-kyr orbital cycles may regulate southward export and upwelling of Circumpolar Deep Water with consequences for melt rates at grounding lines of Antarctic ice sheets. Several recent studies have linked changes in Atlantic meridional overturning[29] and Antarctic circumpolar ocean circulation[30] to obliquity forcing. An interglacial mechanism has been proposed whereby the southward expansion of westerly winds and associated northward Ekman transport is compensated for by enhanced upwelling of warmer, CO_2-rich Circumpolar Deep Water[30], which also promotes atmospheric warming. Such a positive feedback is supported by the strong correlation between temperature and CO_2 in Antarctic ice-core records and may accelerate sea-ice loss with attendant changes in albedo, further increasing oceanic and atmospheric warming.

The low abundance of sea-ice-associated diatoms (<5%) in the early-Pliocene diatomite intervals of the AND-1B cycles suggests that sea surface and air temperatures may have been above freezing for a significant part of the austral summer. On long timescales, insolation integrated over the length of summer (summer energy) has been shown in models to control the surface melting of ice sheets at the obliquity period[8] (Supplementary Information), provided that the ablating margin is at high latitude and that the surface temperature remains above 0 °C for a significant part of the season[31]. Although the latter condition is not currently met by the Antarctic ice sheet, its surface melt threshold may have been exceeded during the early Pliocene and may be exceeded again in the next 100 years. Given the geological evidence from the AND-1B core, we suggest that the mass balance of the early-Pliocene Antarctic ice sheet, although primarily controlled by ocean-induced melting[7], may also have been influenced by surface ablation (Figs 3 and 4). A recent model of the early-Pliocene terrestrial EAIS implies sensitivity to surface temperature on its low-elevation margins at an atmospheric CO_2 level of 400 p.p.m. (ref. 32). Furthermore, documented in-phase insolation-linked warming during an early-Pleistocene interglacial[33] suggests that significant melt may occur during precession-amplified obliquity cycles (Supplementary Information). More well-dated sediment cores, and future experiments using ice-sheet models (see, for example, ref. 7), are planned to assess more fully the different influences of orbital forcing on surface ablation versus ocean-induced melt at elevated atmospheric CO_2 levels.

The unconformity-bounded glacimarine cycles in the AND-1B core provide ice-proximal evidence for ~40-kyr oscillations in Pliocene WAIS and in some of the EAIS outlet glaciers draining into the Ross embayment south of the drill site, a type of behaviour similar to that of the unstable Northern Hemisphere ice sheets of the past ~3 Myr.

METHODS SUMMARY

The 98%-complete AND-1B drill core was recovered from ~850 m of water, from an 85-m-thick portion of the Ross ice shelf, west of Ross Island (Fig. 1 and Supplementary Fig. 1). Drilling used a custom-built riser system embedded into the sea floor, enabling continuous wireline diamond-bit coring to a depth of 1284.87 m.b.s.f. The core was initially processed at the drill site and transported to McMurdo Station on Ross Island where it was split, logged, sampled and analysed. An initial science report provides a summary of drilling, curation and science methods and the initial results that underpin many of the interpretations in this paper[21].

The 38 glacimarine sedimentary cycles are recognized on the basis of the repetitive vertical occurrence of characteristic facies within the AND-1B core. These facies and their interpretations are summarized in Supplementary Table 2, and shown for a single cycle in Supplementary Fig. 3. The age model for the AND-1B core was developed from quantitative diatom biostratigraphic and $^{40}Ar/^{39}Ar$ radiometric ages to constrain the correlation between the magnetic polarity stratigraphy and the geomagnetic polarity timescale. Chronostratigraphic data are summarized in Supplementary Table 1. The biostratigraphic and radiometric datums alone are not used for absolute age control or correlation of cycles with the $\delta^{18}O$ record, because their numeric ages have uncertainties of up to ±50 kyr. However, their precision is sufficient to match polarity zones, identified in the core, with the geomagnetic polarity timescale. These higher-precision (±5 kyr) geomagnetic polarity transitions provide the 'time spikes' for cycle correlation and estimation of cycle duration. For example, the six early-Pliocene glacial cycles between 4.896 and 4.493 Myr ago (Fig. 3) are correlated with C3n.3n/C3n.2r (mid Gilbert, 4.896–4.631 Myr ago) spanning 265 kyr (Fig. 3). Linear interpolation between the dated polarity transitions implies average durations of 39 kyr and 48 kyr per cycle for the lower three (polarity zone N6) and upper three (polarity zone R5) cycles, respectively.

Full Methods and any associated references are available in the online version of the paper at www.nature.com/nature.

Received 25 July 2008; accepted 11 February 2009.

1. Hays, J. D., Imbrie, J. & Shackleton, N. J. Variations in the Earth's orbit; pacemaker of the ice ages. *Science* **194,** 1121–1132 (1976).
2. Raymo, M. E. & Huybers, P. Unlocking the mysteries of the ice ages. *Nature* **415,** 284–285 (2008).
3. Intergovernmental Panel on Climate Change in *Climate Change 2007: The Physical Science Basis. Contribution of Working Group I to the Fourth Assessment Report of the Intergovernmental Panel on Climate Change* (eds Solomon, S. *et al.*) 707–709 (Cambridge Univ. Press, 2007).
4. Kim, S. J. & Crowley, T. J. Increased Pliocene North Atlantic Deep Water: cause or consequence of Pliocene warming. *Paleoceanography* **15,** 451–455 (2000).
5. Van Der Burgh, J., Visscher, H., Dilcher, D. & Kürschner, M. Paleoatmospheric signatures in Neogene fossil leaves. *Science* **260,** 1788–1790 (1993).
6. Raymo, M. E., Grant, B., Horowitz, M. & Rau, G. H. Mid-Pliocene warmth: stronger greenhouse and stronger conveyor. *Mar. Micropaleontol.* **27,** 313–326 (1996).
7. Pollard, D. & DeConto, R. M. Modelling West Antarctic ice sheet growth and collapse through the past five million years. *Nature* (this issue).
8. Huybers, P. Early Pleistocene glacial cycles and the integrated summer insolation forcing. *Science* **313,** 508–511 (2006).
9. Shackleton, N. J. *et al.* Oxygen isotope calibration of the onset of ice-rafting and history of glaciation in the North Atlantic region. *Nature* **307,** 620–623 (1984).
10. Hall, I. R., McCave, I. N., Shackleton, N. J., Weedon, G. P. & Harris, S. E. Intensified deep Pacific inflow and ventilation in Pleistocene glacial times. *Nature* **412,** 809–812 (2001).
11. Crundwell, M., Scott, G., Naish, T. R. & Carter, L. Glacial–interglacial ocean-climate variability spanning the Mid-Pleistocene transition in the temperate Southwest Pacific, ODP site 1123. *Palaeogeogr. Palaeoclimatol. Palaeoecol.* **260,** 202–229 (2008).
12. Dwyer, G., Baker, P. & Cronin, T. North Atlantic deepwater temperature change during late Pliocene and late Quaternary climatic cycles. *Science* **270,** 1347–1350 (1995).
13. Ding, Z. L. *et al.* Stacked 2.6-Ma grain size record from the Chinese loess based on five sections and correlation with the deep-sea $\delta^{18}O$ record. *Paleoceanography* **17,** 5–21 (2002).
14. Naish, T. R. Constraints on the amplitude of late Pliocene eustatic sea-level fluctuations: new evidence from the New Zealand shallow-marine sediment record. *Geology* **25,** 1139–1142 (2007).
15. Raymo, M. E., Lisiecki, L. & Nisancioglu, K. Plio–Pleistocene ice volume, Antarctic climate, and the global $\delta^{18}O$ record. *Science* **313,** 492–495 (2006).
16. Mercer, J. H. West Antarctic ice sheet and CO_2 greenhouse effect: a threat of disaster. *Nature* **271,** 321–325 (1978).
17. Dowsett, J. & Cronin, T. M. High eustatic sea level during the middle Pliocene: evidence from the southeastern U.S. Atlantic Coastal Plain. *Geology* **18,** 435–438 (1990).
18. Naish, T. R. & Wilson, G. Constraints on the amplitude of Mid-Pliocene (3.6–2.4 Ma) eustatic sea-level fluctuations from the New Zealand shallow-marine sediment record. *Phil. Trans. R. Soc. A* **367,** 169–187 (2009).
19. Kennett, J. P. & Hodell, D. A. Evidence for relative climatic stability of Antarctica during the Early Pliocene: A marine perspective. *Geogr. Ann.* **75A,** 202–222 (1993).
20. Naish, T. R. *et al.* in *Antarctica: A Keystone in a Changing World* (eds Cooper, A. K. *et al.*) 71–82 (Proc. 10th Internat. Symp. Antarctic Earth Sci., National Academies Press, 2008).
21. Naish, T. R., Powell, R. D. & Levy, R. H. (eds) *Studies from the ANDRILL, McMurdo Ice Shelf Project, Antarctica - Initial Science Report on AND-1B* (Terra Antartica Vol. 14, 2007).
22. Dunbar, G., Naish, T. R., Powell, R. D. & Barrett, P. J. Constraining the amplitude of late Oligocene bathymetric changes in western Ross Sea during orbitally-induced oscillations in the East Antarctic Ice Sheet: (1) Implications for glacimarine sequence stratigraphic model. *Palaeogeogr. Palaeoclimatol. Palaeoecol.* **260,** 50–65 (2008).

23. Powell, R. D. & Cooper, J. M. A sequence stratigraphic model for temperate, glaciated continental shelves. *Spec. Publ. Geol. Soc. (Lond.)* **203,** 215–244 (2003).
24. Lewis, A. R. *et al.* Mid-Miocene cooling and the extinction of tundra in continental Antarctica. *Proc. Natl Acad. Sci. USA* **105,** 10676–10689 (2008).
25. Naish, T. R., Carter, L., Wolff, E., Pollard, D. & Powell, R. D. in *Developments in Earth & Environmental Sciences* Vol. 8 (eds Florindo, F. & Seigert M.) 465–529 (Elsevier, 2009).
26. Lisiecki, L. E. & Raymo, M. E. A. Pliocene-Pleistocene stack of 57 globally distributed benthic $\delta^{18}O$ records. *Paleoceanography* **20,** doi:10.1029/2005PA001153 (2005).
27. McKay, R. *et al.* Retreat of the Ross Ice Shelf since the Last Glacial Maximum derived from sediment cores in deep basins surrounding Ross Island. *Palaeogeogr. Palaeoclimatol. Palaeoecol.* **260,** 245–261 (2008).
28. Young, M. & Bradley, R. in *Milankovitch and Climate* (eds Berger, A. *et al.*) 707–713 (Riedel, 1984).
29. Lisiecki, L. E., Raymo, M. E. & Curry, W. B. Atlantic overturning responses to Late Pleistocene climate forcings. *Nature* **456,** 85–88 (2008).
30. Toggweiler, J. R., Russell, J. L. & Carson, S. R. Mid-latitude westerlies, atmospheric CO_2, and climate change. *Paleoceanography* **21,** doi:10.1029/2005PA001154 (2007).
31. Huybers, P. & Tziperman, E. Integrated summer insolation forcing and 40,000-year glacial cycles: the perspective from an ice-sheet/energy-balance model. *Paleoceanography* **23,** doi:10.1029/2007PA001463 (2008).
32. Hill, D. J., Haywood, A. M., Hindmarsh, R. C. A. & Valdes, P. J. in *Deep Time Perspectives on Climate Change: Marrying the Signals from Computer Models and Biological Proxies* (eds Williams, M. *et al.*) 517–538 (Micropalaeontol. Soc. Spec. Publ., Geological Society of London, 2007).
33. Scherer, R. P. *et al.* Antarctic records of precession paced, insolation-driven warming during the early Pleistocene Marine Isotope Stage 31. *Geophys. Res. Lett.* **35,** doi:10.1029/2007gl032254 (2008).

Supplementary Information is linked to the online version of the paper at www.nature.com/nature.

Acknowledgements The ANDRILL project is a multinational collaboration between the Antarctic programmes of Germany, Italy, New Zealand and the United States. Antarctica New Zealand is the project operator and developed the drilling system in collaboration with A. Pyne. Antarctica New Zealand supported the drilling team at Scott Base; Raytheon Polar Services Corporation supported the science team at McMurdo Station and the Crary Science and Engineering Laboratory. The ANDRILL Science Management Office at the University of Nebraska-Lincoln provided science planning and operational support. The scientific studies are jointly supported by the US National Science Foundation, the New Zealand Foundation for Research Science and Technology and the Royal Society of New Zealand Marsden Fund, the Italian Antarctic Research Programme, the German Research Foundation and the Alfred Wegener Institute for Polar and Marine Research.

Author Contributions All authors contributed to acquisition, analysis and interpretation of data presented in this paper. T.N.: overall coordination of writing, sedimentology, cyclostratigraphic and climatic interpretations; R.P.: integration, glacial facies, glacial process and interpretations of ice-sheet history; R.L.: integration, biochronology and age-model construction; L.K.: core description and sedimentological interpretation; F.N.: core description and physical properties interpretation; M.P.: petrological interpretation; R.S.: integration, diatom biostratigraphic and environmental interpretations; F.T.: clast abundance, composition and provenance interpretations; G.W.: palaeomagnetic stratigraphy and age-model construction; T. Wilson: core description, structural and tectonic constraints; L.C.: sedimentology & palaeo-oceanographic interpretations; R. McKay: sedimentology, glacial facies interpretations and ice-sheet history; J. Ross: $^{40}A/^{39}Ar$ geochronology and age-model construction; D.W.: diatom biostratigraphy and environmental interpretations; P.B.: glacial process and interpretations of ice-sheet history; G.B.: glacimarine sequence stratigraphy and facies interpretations; R.C.: biochronology and age-model construction; E.C.: glacial facies, glacial process and interpretations of ice-sheet history; J.C.: biochronology and age-model construction; R.D.: ice-sheet-model data interpretation and integration; G.D.: core description, facies and sedimentological interpretation; N.D.: $^{40}Ar/^{39}Ar$ geochronology and petrological interpretation; F.F.: palaeomagnetic interpretations and age-model construction; C.G.: core description and physical properties interpretation; I.G.: geochronology and age-model construction; M.H.: biostratigraphy and environmental interpretation; D. Harwood: diatom biostratigraphy and biochronology; D. Hansaraj: regional seismic stratigraphic context; D. Helling: geochemical interpretation; S.H.: regional stratigraphic framework and tectonic constraints; L.H.: time-series analysis; P.H.: Milankovitch forcing and palaeoclimatic interpretations; G.K.: geochemical interpretation; P.K.: volcanic petrology and volcanological interpretation; A.L.: core description and structural analysis; P.M.: diatom biostratigraphy and environmental interpretations; D.M.: core description and physical properties interpretation; K.M.: core description; W.M.: $^{40}Ar/^{39}Ar$ geochronology and volcanological interpretation; C.M.: core description and structural analysis; R. Morin: borehole description and down-hole geophysics; C.O.: palaeomagnetic stratigraphy and age-model construction; T.P.: core and description and structural geology; D. Persico: calcareous nannofossil biostratigraphy; D. Pollard: ice-sheet-model data interpretation and integration; J. Reed: core description and visualization; C.R.: diatom biostratigraphy and environmental interpretation; I.R.: palynology and environmental interpretation; D.S.: core and borehole description and structural geology; L.S.: palaeomagnetic stratigraphy and age-model construction; C.S.: diatom biostratigraphy and environmental interpretation; P.S.: foram biostratigraphy and environmental interpretation; M.T.: macrofossil biostratigraphy and environmental interpretation; S.V.: subglacial geological interpretation; T. Wilch: core description and interpretation of volcaniclastic sediments; T. Williams: borehole description and down-hole geophysics.

Author Information Reprints and permissions information is available at www.nature.com/reprints. Correspondence and requests for materials should be addressed to T.N. (tim.naish@vuw.ac.nz).

METHODS

Facies analysis of sedimentary cycles and the interpretation of glacial proximity. The individual glacimarine cycles are interpreted to represent ice advance–retreat–re-advance of the grounding line of a laterally continuous ice sheet in Ross embayment, and (from bottom to top) include the following stratigraphic elements.

(1) Erosion and subglacial deposition by an advancing ice sheet producing a GSE that is sharp, planar to sub-horizontal and truncates underlying deposits. Syndepositional soft-sediment deformation structures, intraclasts, clastic dykes and shearing of lithologies occur above and below the GSE. Subglacial features are also indicated by clast orientation and striation within tills.

(2) An interval of grounding-zone deposition comprising conglomerates and poorly sorted stratified sandstones together with stratified diamictite represent a range of basal meltwater conditions observed from subpolar to polar environments[34], and are associated with glacimarine processes including subglacial meltwater outwash, proglacial debris-flow deposition, and iceberg rainout. These pass upwards into finer-grained terrigenous sediments representing more distal deposition from turbid plumes and grounding-line fans as the grounding line continues to retreat[35,36]. In some cases, ice-shelf environments are indicated by non-fossiliferous, unbioturbated intervals of interstratified sands and silts occurring stratigraphically between ice-proximal and open-marine facies[37].

(3) Open-marine hemipelagic and pelagic sedimentation with and without iceberg influence. The distal deposits with least glacial influence are diatomites representing biogenic sediment accumulation in an ice-free, highly productive ocean setting.

(4) A proglacial facies succession of progressively more proximal grounding-zone deposits (as in (2)), represents ice-sheet re-advance and eventual glacial overriding at the drill site. This may or may not be preserved below the GSE, depending on the degree of erosion on the GSE.

Several facies commonly associated with proximal glacimarine deposition are noted in AND-1B (Supplementary Table 2), including mudstone with dispersed clasts, conglomerates, sorted sandstone (with a TAM provenance), conglomerates and rhythmically interlaminated couplets of claystone with either siltstone or very fine-grained sandstone (see, for example, Supplementary Fig. 3). The changing abundance of these facies throughout the core, and comparison with modern-day analogues, provides insight into the past extent of subglacial meltwater processes following the concepts established for the Cape Roberts Project core[38]. For example, the rhythmically interlaminated claystone with silt/sandstone facies in AND-1B are consistent with previously described cyclopsam and cyclopel facies from modern temperate to subpolar glacimarine environments in Alaska and the Greenland margin, where they are deposited in quiet-water basins by suspension settling from meltwater plumes[35,36]. These sediments are unknown in modern-day Antarctic glacimarine settings, yet are common in temperate to subpolar settings[39].

Chronostratigraphic constraints. A preliminary age model for the upper 600 m of the drill core constructed from diatom biostratigraphy, and radiometric ages on volcanic material, allows a unique correlation of ~36% of the magnetic polarity stratigraphy with the geomagnetic polarity timescale. Since publication of this age model[21], the chronology has been improved by further diatom biostratigraphic analysis of the diatomite interval between 460 and 383 m.b.s.f. We now identify a significant hiatus of ~800 kyr at the base of a volcaniclastic gravity-flow deposit at ~440.12 m.b.s.f. Additionally, a new $^{40}Ar/^{39}Ar$ potassium feldspar age of 4.800 ± 0.076 Myr on a primary volcanic deposit at 481.80 m.b.s.f. (Supplementary Information) confirms the correlation of our magnetic polarity stratigraphy with the geomagnetic polarity timescale for this early-Pliocene interval of the core. All chronostratigraphic datums used to constrain estimates of cycle duration, and correlations with proxy climate and climate-forcing time series in Fig. 2 and Supplementary Fig. 4 for the upper 600 m of the AND-1B core, are summarized in Supplementary Table 1.

Early-Pliocene chronostratigraphy between 400 and 600 m.b.s.f. Biostratigraphic event ages include the maximum and minimum ages identified in the CONOP constrained Southern Ocean diatom biochronologic calibration of ref. 40. The ages for new events described below are determined from recent model runs[41]. The first occurrence of *Rhizosolenia* sp. D is observed at 440.12 m.b.s.f. The maximum age of this event is well constrained in the latest versions of the CONOP models (which incorporate AND-1B data). *Rhizosolenia* sp. D has been documented in at least seven sections from around the Antarctic[40]. The occurrence of this diatom event, therefore, requires the age of the core at and above 440.12 m.b.s.f. to be <3.58 Myr. The palaeomagnetic zone in this portion of the core (440.12–346.13 m.b.s.f.) is normal and correlates C2An.3n (base of the Gauss chron, 3.596–3.300 Myr ago). The absence of *Fragilariopsis interfrigidaria* and *Fragilariopsis barronii* between 450 and 440.12 m.b.s.f. implies an age-range equivalent depth of 4.72–4.29 m.b.s.f. for this interval and constrains the minimum duration of the unconformity below 440.12 m.b.s.f. to ~800 kyr. The first occurrence of *Thalassiosira striata* is observed at 456.00 m.b.s.f., constraining the maximum age of the core at this level to 4.78 Myr and identifying the short normal-polarity interval between 459.19 and 452.86 m.b.s.f. as the Nunivak subchron (C3n.2n, 4.631–4.493 Myr ago). The radiometric age of 4.8 ± 0.076 Myr on the pumice-rich layer at 481.8 m.b.s.f. constrains the superjacent N–R transition at 519.4 m.b.s.f. to the top of the Sidufjall subchron (4.799 Myr ago). The first occurrence of the marine diatom *Thalassiosira complicata* at 583.64 m.b.s.f. is 4.86 Myr ago and constrains correlation of the R–N transition at 596.35 m.b.s.f. with the base of the Sidufjall subchron (4.896 Myr ago).

Calibration of the benthic foraminiferal $\delta^{18}O$ curve to sea level. The stacked benthic foraminiferal $\delta^{18}O$ record for the last 5 Myr (ref. 25) was converted to a sea-level curve by scaling with a calibration of 0.011‰ m^{-1}, which is consistent with ice-volume $\delta^{18}O$ calibrations derived from a number of sources: uplifted Late Quaternary remnant shorelines[42], equatorial planktonic foraminiferal isotope records with minimal temperature influence[43] and back-stripped estimates of eustatic sea level from continental margin sequences[14,44]. The calibration removes a consistent 20% temperature contribution from the total amplitude of glacial–interglacial isotopic variation. For example, the LGM-to-Holocene shift in the stacked isotope curve of 1.7‰, when calibrated to the corresponding sea-level shift estimated from Huon Peninsula palaeoshoreline sequence, is 1.2–1.3‰ or 0.011‰ m^{-1}. The difference is due to glacial–interglacial deep-ocean temperature changes of 2 °C or 0.3–0.4‰.

34. Dowdeswell, J. A., Elverhøi, A. & Spielhagen, R. Glacimarine sedimentary processes and facies on the Polar North Atlantic margins. *Quat. Sci. Rev.* **17**, 243–272 (1998).
35. Ó Cofaigh, C., &. Dowdeswell, J. A. Laminated sediments in glacimarine environments: diagnostic criteria for their interpretation. *Quat. Sci. Rev.* **20**, 1411–1436 (2001).
36. Cowan, E. A., Seramur, K. C., Cai, J. & Powell, R. D. Cyclic sedimentation produced by fluctuations in meltwater discharge, tides and marine productivity in an Alaskan fjord. *Sedimentology* **46**, 1109–1126 (1999).
37. Domack, E. W., Jacobson, E. A., Shipp, S. & Anderson, J. B. Late Pleistocene-Holocene retreat of the West Antarctic ice-sheet system in the Ross Sea, Part 2: Sedimentologic and stratigraphic signature. *Geol. Soc. Am. Bull.* **111**, 1517–1536 (1999).
38. Powell, R. D. *et al.* Facies analysis and depositional environments in CRP-3: implications for Oligocene glacial history. *Terra Antartica* **8**, 207–217 (2001).
39. Powell, R. D. & Domack, E. W. in *Modern and Past Glacial Environments* (ed. Menzies, J.) Ch. 12, 361–389 (Butterworth-Heinemann, 2002).
40. Cody, R., Levy, R., Harwood, D. & Sadler, P. Thinking outside the zone: high-resolution quantitative biochronology for the Antarctic Neogene. *Palaeogeogr. Palaeoclimatol. Palaeoecol.* **260**, 92–121 (2008).
41. Cody, R, *et al.* Quantitative biostratigraphic modelling of the AND-1B drillcore. *Glob. Planet. Change* (submitted).
42. Chappell, J. *et al.* Reconciliation of Late Quaternary sea levels derived from coral terraces at Huon Peninsula with deep sea oxygen isotope records. *Earth Planet. Sci. Lett.* **141**, 227–236 (1996).
43. Tiedemann, R., Sarnthein, M. & Shackleton, N. J. Astronomical timescale for the Pliocene Atlantic $\delta^{18}O$ and dust flux records of Ocean Drilling Program Site 659. *Paleoceanography* **9**, 619–638 (1994).
44. Miller, K. G. *et al.* The Phanerozoic record of global sea-level change. *Science* **310**, 1293–1298 (2005).